3-15-2021

On IP2 Impact to Nonlinear Distortion of RF Amplifiers

Xianzhen Yang
Portland State University, xianzhen@pdx.edu

Shiyu Li
Portland State University

Siyuan Yan
Portland State University

Fu Li
Portland State University, if@pdx.edu

Citation Details

Yang, X., Li, S., Yan, S., & Li, F. (2021). On IP2 impact to nonlinear distortion of RF amplifiers. *The Journal of Engineering*, tje2.12028. https://doi.org/10.1049/tje2.12028

Received: 24 December 2020 | Revised: 2 February 2021 | Accepted: 17 February 2021

The Journal of Engineering

DOI: 10.1049/tje2.12028

The Institution of Engineering and Technology WILEY

ORIGINAL RESEARCH PAPER

On IP2 impact to nonlinear distortion of RF amplifiers

Xianzhen Yang | **Shiyu Li** | **Siyuan Yan** | **Fu Li**

Department of Electrical and Computer Engineering, Portland State University, Portland, Oregon, USA

Correspondence
Fu Li, Department of Electrical and Computer Engineering, Portland State University, 1900 SW 4th Avenue, Suite 160-10, Portland, OR 97207-0751, USA.
Email: lif@pdx.edu

Abstract

The second-order distortion, often using second-order intercept point (IP2) as an indicator, has been considered easy to be filtered in narrowband radio frequency (RF) communications because it is located far away from the passband of transmitted signals. However, with rapidly increased applications in wideband RF communications, the second-order intermodulation (IM) might become important, partially evidenced by the increased appearances of IP2 in the amplifier datasheets in recent years. In this article, a power spectrum model of the second-order IM is derived to quantify the second-order distortion using the IP2. This model could be used to determine under what conditions, in terms of the relation between the carrier frequency and bandwidth, the second-order IM will affect the passband or the adjacent bands or other applications, using three types of frequency scenarios. These discussions are beneficial for RF engineers and spectrum planners to predict interferences from second-order IM. The experimental measurement at the end of the article validates the spectrum model.

1 | INTRODUCTION

Radio frequency (RF) amplifiers are important components in wireless communication systems. The non-linearities of RF amplifiers will affect the system spectrum performances. Taylor series model has been widely used to represent memoryless non-linearities of RF amplifiers. Generally, the even-order distortion terms will be far away from the passband and are of less concern than the odd-order distortion terms [1]. Neglecting the even-order terms is usually applied to narrowband RF communications, which are defined as the bandwidth is far less than the centre frequency.

However, recent studies suggested that the second-order intermodulation (IM) distortion may be significant in wideband transceivers widely used in long-term evolution advanced (LTE-A) and fifth-generation new radio (5G NR) systems [2–7]. In direct conversion receivers, also known as homodyne or zero-IF receivers, the second-order IM dominates in degrading the performance of the receiver by causing a severe signal-to-interference-plus-noise ratio degradation of the received signal [6, 7] because the regenerated second-order distortion is hard to discriminate from the desired signal [8]. Further, the second-order intercept point (IP2), which is used to quantify the second-order distortion regenerated by non-linear systems and devices, appears more frequently in recent amplifier datasheets [9].

In this article, a power spectrum model of the second-order IM products based on IP2 and other parameters, such as gain, carrier frequency, and bandwidth, is derived. This model is then used to analyse under what conditions the second-order IM will affect the passband and adjacent bands through the wideband power amplifier operation using three types of frequency scenarios. The experimental measurement validates the power spectrum model of second-order IM. The power spectrum model can help RF engineers, spectrum planners and regulators to predict and forecast the potential second-order interferences, particularly for 5G NR, LTE-A, and other wideband applications.

2 | POWER SPECTRUM OF SECOND-ORDER IM

The Taylor series is one of the popular polynomial models of amplifiers and can be expressed as

$$y(t) = a_1 s(t) + a_2 s^2(t) + \cdots + a_n s^n(t) + \cdots \quad (1)$$

where a_n is the Taylor coefficient of the n^{th} order term, $s(t)$ is the input signal, $y(t)$ is the output signal. Traditionally, only odd-order terms in Equation (1) are considered [1] because the even-order terms are generally far away. Due to the increasingly popular wideband amplifications, we now include even-order terms, specifically the second-order term, into consideration.

In this article, we use OFDM signal as the input signal, which in passband can be represented as

$$s(t) = \text{Re}\left\{g(t)\, e^{j2\pi f_c t}\right\} = \tilde{s}(t)\cos\left[2\pi f_c t + \theta(t)\right] \tag{2}$$

where Re{•} denotes the real part of {•}, $g(t)$ is the complex envelope of $s(t)$, f_c is the carrier frequency, $\tilde{s}(t)$ is the magnitude of $g(t)$, and $\theta(t)$ is the phase of $g(t)$. The power spectral density (PSD) of $\tilde{s}(t)$ is given below [10]:

$$P_{\tilde{s}}(f) = \begin{cases} \frac{N_0}{2}, & |f| \le B \\ 0, & |f| > B \end{cases} \tag{3}$$

where B is the bandwidth, and $N_0 B$ is the power of $\tilde{s}(t)$.

Based on [11, eq. (4–11)–(4–13)], the power spectrum of the passband waveform in Equation (2) is

$$P_s(f) = \frac{1}{4}\left[P_{\tilde{s}}(f - f_c) + P_{\tilde{s}}(-f - f_c)\right] \tag{4}$$

where $P_s(f)$ and $P_{\tilde{s}}(f)$ denote the power spectrum of $s(t)$ and $\tilde{s}(t)$, respectively. It is noticeable that the $\theta(t)$ in Equation (2) does not affect the power spectrum in Equation (4). As we will derive the PSD model using Equation (4) in this article, $\theta(t)$ could be dropped from Equation (2). Thus, Equation (2) can be rewritten as

$$s(t) = \tilde{s}(t)\cos\left(2\pi f_c t\right) \tag{5}$$

Again, note that Equation (5) is only valid when we develop PSD. Among all the even-order terms of the Taylor series, the second-order term dominates. Therefore, we will only consider the second-order term in this article. Because the input power is relatively low, it is possible to ignore all the high-order ($n > 3$) IM. Considering the Taylor series up to the third-order (i.e. $n = 3$) with an assumption of weak non-linearity and substituting Equations (5) into (1), the amplified signal is derived as

$$\begin{aligned} y(t) = {} & a_1\tilde{s}(t)\cos\left(2\pi f_c t\right) + a_2\left[\tilde{s}(t)\cos\left(2\pi f_c t\right)\right]^2 \\ & + a_3\left[\tilde{s}(t)\cos\left(2\pi f_c t\right)\right]^3 \end{aligned} \tag{6}$$

After derivation using trigonometric identities, Equation (6) can be expressed as

$$\begin{aligned} y(t) = {} & \frac{1}{2}a_2\tilde{s}^2(t) + \left[a_1\tilde{s}(t) + \frac{3}{4}a_3\tilde{s}^3(t)\right]\cos\left(2\pi f_c t\right) \\ & + \frac{1}{2}a_2\tilde{s}^2(t)\cos\left(4\pi f_c t\right) + \frac{1}{4}a_3\tilde{s}^3(t)\cos\left(6\pi f_c t\right) \end{aligned} \tag{7}$$

To simplify Equation (7) for future derivations, we define

$$\bar{y}_1(t) = \frac{1}{2}a_2\tilde{s}^2(t) \tag{8}$$

$$\bar{y}_2(t) = a_1\tilde{s}(t) + \frac{3}{4}a_3\tilde{s}^3(t) \tag{9}$$

$$\bar{y}_3(t) = \frac{1}{4}a_3\tilde{s}^3(t) \tag{10}$$

Equation (7) then can be rewritten as

$$\begin{aligned} y(t) = {} & \bar{y}_1(t) + \bar{y}_2(t)\cos\left(2\pi f_c t\right) \\ & + \bar{y}_1(t)\cos\left(4\pi f_c t\right) + \bar{y}_3(t)\cos\left(6\pi f_c t\right) \end{aligned} \tag{11}$$

The first and third terms in Equation (11) denote the second-order IM centred around DC and second-order harmonic frequency $2f_c$, respectively, the second term in Equation (11) is the transmitted signal together with the third-order IM centred around the carrier frequency f_c, and the fourth term in Equation (11) represents the third-order IM centred around the third-order harmonic frequency $3f_c$. We will consider only the power spectrum derivation of the third term in this article because the power spectrums of the first and third terms are symmetric, the second term was discussed by previous researchers [12], the fourth term is located far away from the band of interest and is thus filtered. Therefore, the second-order IM $y_1(t)$ is expressed as

$$y_1(t) = \bar{y}_1(t)\cos\left(4\pi f_c t\right) \tag{12}$$

Denoting the power spectrum of $\bar{y}_1(t)$ as $P_{\bar{y}_1}(f)$, the power spectrum of $y_1(t)$ can be expressed as

$$P_{y_1}(f) = \frac{1}{4}\left[P_{\bar{y}_1}(f - 2f_c) + P_{\bar{y}_1}(-f - 2f_c)\right] \tag{13}$$

Equation (13) is symmetric in frequency. In the real-time measurement, only the spectrum in the positive frequency range is measurable with twice the magnitude. Therefore, Equation (13) can be rewritten as

$$P_{y_1}(f) = \frac{1}{2}\left[P_{\bar{y}_1}(f - 2f_c)\right] \tag{14}$$

For simplicity, we will use Equation (14) in the rest of this article. According to the Wiener–Khintchine theorem, the power spectrum $P_{\bar{y}_1}(f)$ can be related to the autocorrelation function $R_{\bar{y}_1}(\tau)$ of $\bar{y}_1(t)$ by

$$P_{\bar{y}_1}(f) = \mathcal{F}\left\{R_{\bar{y}_1}(\tau)\right\} = \int_{-\infty}^{\infty} R_{\bar{y}_1}(\tau)\, e^{-j2\pi f\tau} d\tau \tag{15}$$

where $\mathcal{F}\{\bullet\}$ denotes the Fourier transform of {•}.

By the definition of autocorrelation, $R_{\bar{y}_1}(\tau)$is expressed as

$$R_{\bar{y}_1}(\tau) = \mathcal{E}\left\{\bar{y}_1(t)\bar{y}_1(t+\tau)\right\} \tag{16}$$

where $\mathcal{E}\{\bullet\}$ is the mathematical expectation of $\{\bullet\}$.

Equation (16) can be further expressed in terms of $\tilde{s}(t)$ as

$$\begin{aligned} R_{\tilde{y}_1}(\tau) &= \mathcal{E}\{\tilde{y}_1(t)\tilde{y}_1(t+\tau)\} \\ &= \mathcal{E}\left\{\frac{1}{2}a_2\tilde{s}^2(t)\frac{1}{2}a_2\tilde{s}^2(t+\tau)\right\} \\ &= \frac{1}{4}a_2^2\mathcal{E}\left\{\tilde{s}^2(t)\tilde{s}^2(t+\tau)\right\} \end{aligned} \tag{17}$$

The mathematical expectation of $\tilde{s}^2(t)\tilde{s}^2(t+\tau)$ can be calculated by the Isserlis' theorem [13] as

$$\begin{aligned} \mathcal{E}\left\{\tilde{s}^2(t)\tilde{s}^2(t+\tau)\right\} &= \mathcal{E}\{\tilde{s}(t)\tilde{s}(t)\}\mathcal{E}\{\tilde{s}(t+\tau)\tilde{s}(t+\tau)\} \\ &\quad + 2[\mathcal{E}\{\tilde{s}(t)\tilde{s}(t+\tau)\}]^2 \end{aligned} \tag{18}$$

In Equation (18), the expectation of $\tilde{s}(t)\tilde{s}(t+\tau)$ is the autocorrelation of $\tilde{s}(t)$, which could be derived from the inverse Fourier transform of $P_{\tilde{s}}(f)$ in Equation (2) as

$$\begin{aligned} \mathcal{E}\{\tilde{s}(t)\tilde{s}(t+\tau)\} &= R_{\tilde{s}}(\tau) = \mathcal{F}^{-1}\left\{P_{\tilde{s}}(f)\right\} \\ &= N_0 B\frac{\sin(2\pi B\tau)}{2\pi B\tau} \end{aligned} \tag{19}$$

By substituting $\tau = 0$ into Equation (19), the expectation of $\tilde{s}(t)\tilde{s}(t)$ and $\tilde{s}(t+\tau)\tilde{s}(t+\tau)$ can be derived as

$$\mathcal{E}\{\tilde{s}(t)\tilde{s}(t)\} = \mathcal{E}\{\tilde{s}(t+\tau)\tilde{s}(t+\tau)\} = N_0 B \tag{20}$$

Substituting Equations (19) and (20) into (18), the expectation of $\tilde{s}^2(t)\tilde{s}^2(t+\tau)$ can be simplified as

$$\mathcal{E}\left\{\tilde{s}^2(t)\tilde{s}^2(t+\tau)\right\} = (N_0B)^2 + 2\left[N_0B\frac{\sin(2\pi B\tau)}{2\pi B\tau}\right]^2 \tag{21}$$

Thus, Equation (17) can be further expressed as

$$\begin{aligned} R_{\tilde{y}_1}(\tau) &= \frac{1}{4}a_2^2\left\{(N_0B)^2 + 2\left[N_0B\frac{\sin(2\pi B\tau)}{2\pi B\tau}\right]^2\right\} \\ &= \frac{1}{4}a_2^2N_0^2B^2 + \frac{1}{2}a_2^2R_{\tilde{s}}^2(\tau) \end{aligned} \tag{22}$$

Substituting Equations (22) into (15), the power spectrum $P_{\tilde{y}_1}(f)$ can be calculated as

$$\begin{aligned} P_{\tilde{y}_1}(f) &= \mathcal{F}\left\{R_{\tilde{y}_1}(\tau)\right\} = \mathcal{F}\left\{\frac{1}{4}a_2^2N_0^2B^2 + \frac{1}{2}a_2^2R_{\tilde{s}}^2(\tau)\right\} \\ &= \begin{cases} \frac{1}{4}a_2^2N_0^2B^2\delta(f) + \frac{1}{8}a_2^2N_0^2(2B-|f|), & |f| \le 2B \\ 0, & |f| > 2B \end{cases} \end{aligned} \tag{23}$$

To express Equation (23) in terms of gain (G) and third-order IP, which are easier to use from the datasheet, some relationships are introduced [14],

$$a_1 = 10^{\frac{G}{20}} \tag{24}$$

$$a_2^2 = \frac{1}{2}10^{\left(\frac{-IP_2}{10}+\frac{G}{5}\right)} \tag{25}$$

Thus, the power spectrum of $P_{\tilde{y}_1}(f)$ can be rewritten as

$$P_{\tilde{y}_1}(f) = \begin{cases} \frac{1}{2}10^{\left(\frac{-IP_2}{10}\right)}P_0^2\delta(f) \\ \quad + \frac{1}{4B^2}10^{\left(\frac{-IP_2}{10}\right)}P_0^2(2B-|f|), & |f| \le 2B \\ 0, & |f| > 2B \end{cases} \tag{26}$$

where $P_0 = a_1^2N_0B/2$ is the linear output power of the RF amplifier.

By substituting Equations (26) into (14), the power spectrum of the second-order IM can be expressed as

$$P_{\tilde{y}_1}(f) = \begin{cases} \frac{1}{4}10^{\left(\frac{-IP_2}{10}\right)}P_0^2\delta(f-2f_c) \\ \quad + \frac{1}{8B^2}10^{\left(\frac{-IP_2}{10}\right)}P_0^2(2B-|f-2f_c|), & |f-2f_c| \le 2B \\ 0, & |f-2f_c| > 2B \end{cases} \tag{27}$$

An illustration of Equation (27) is shown in Figure 1. The parameters are set as follows, $f_c = 930$MHz in 5G downlink band n8 [15], $B = 5$ MHz, $IP_2 = 38.69$dBm, and $P_0 = 1.5$dBm. This will be verified in the later section of the experiment.

In the most recent applications, such as 4G, LTE, and Wi-Fi, the carrier frequency f_c is usually far larger than the bandwidth B. In this condition, the second-order IM, which is centred around $2f_c$, is far away from the band of interest and is easy to be filtered. However, when f_c is not far greater than B, the second-order IM could impact or even overlap with the carrier band and/or adjacent bands or other applications.

To explore the scenarios where the second-order IM would affect the passband and adjacent bands, we need to use the power spectrum expression of the signals in those bands. This spectrum expression $P_{\tilde{y}_2}(f)$ was developed in [12] and is shown as

$$P_{\tilde{y}_2}(f) = \begin{cases} \frac{1}{2B}\left[P_0 - 6P_0^210^{\left(\frac{-IP_3}{10}\right)} + 9P_0^310^{\left(\frac{-IP_3}{5}\right)}\right] \\ \quad + \frac{3}{4B^3}P_0^310^{\left(\frac{-IP_3}{5}\right)}\left[3B^2 - (f-f_c)^2\right], & |f-f_c| \le B \\ \frac{3}{8B^3}P_0^310^{\left(\frac{-IP_3}{5}\right)}(3B-|f-f_c|)^2, & B < |f-f_c| \le 3B \\ 0, & |f-f_c| > B \end{cases} \tag{28}$$

The first frequency segment in Equation (28) describes the power spectrum within the passband, and the second segment in Equation (28) shows the third-order regrowth located in the adjacent channels. From Equation (28), we can observe that the

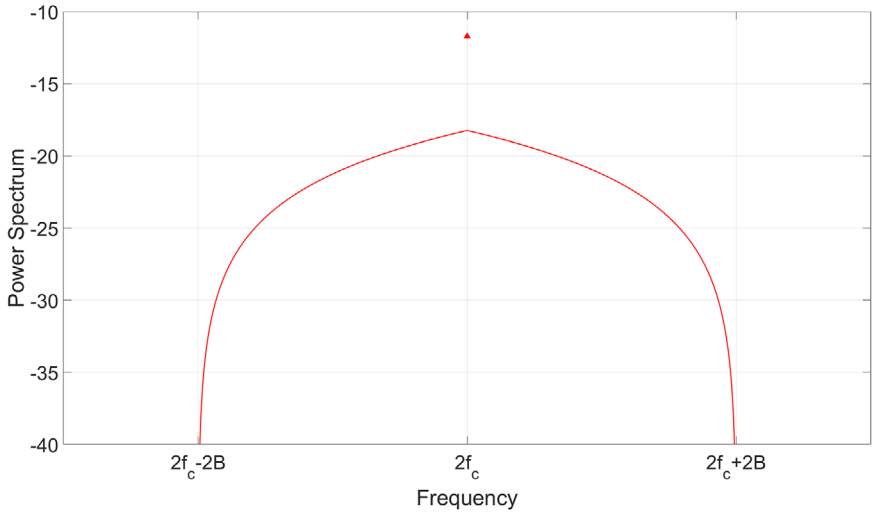

FIGURE 1 Power spectrum of $P_{y_1}(f)$

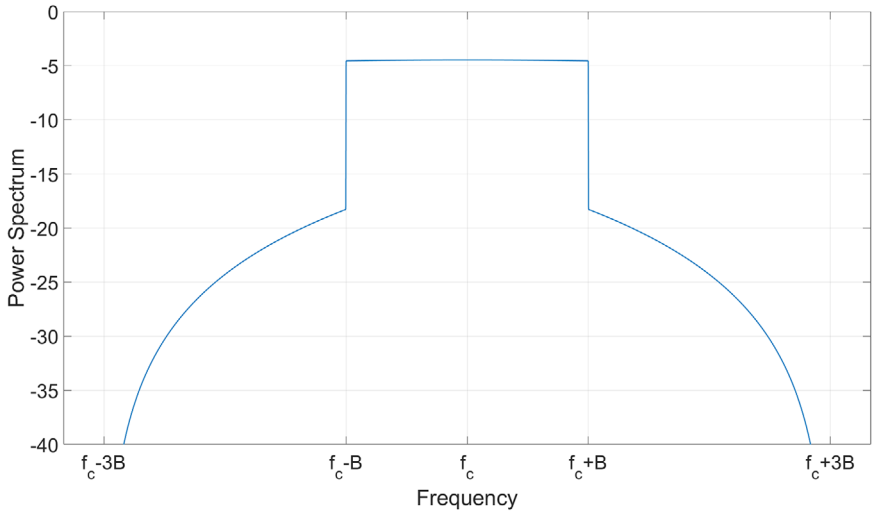

FIGURE 2 Power spectrum of $P_{y_2}(f)$

third-order IM not only generates regrowth in adjacent channels but also degrades signal quality in the passband channel. An illustration figure of $P_{y_2}(f)$ is shown in Figure 2. IP_3 is set as 26.12 dBm, which is shown in the datasheet of the amplifier ZX60-8008E+ that we used in the experiment section. The other parameters are the same as in Figure 1.

From Equations (27) and (28), we can see that the second-order IM is located in the frequency range from $(2f_c - 2B)$ to $(2f_c + 2B)$, while the passband and third-order regrowth are located in the frequency range from $(f_c - 3B)$ to $(f_c + 3B)$. The impact of the second-order IM will be discussed in three frequency scenarios in terms of the relation between centre frequency f_c and bandwidth B in the next section.

3 | FREQUENCY SCENARIOS OF SECOND-ORDER IM

3.1 | Frequency scenario 1

$$f_c > 5B \tag{29}$$

The inequality comes from $2f_c - 2B > f_c + 3B$. This is probably the most common condition in RF communications while the second-order IM has no effects on the passband or adjacent bands. In fact, the centre frequency is far greater than bandwidth ($f_c \gg 5B$). An illustration of scenario 1 is shown in Figure 3.

In Figure 3, the blue waveform represents Equation (28), and the red waveform represents Equation (27), which is the same as the following Figures 4 and 5. We can observe that the left edge of the second-order IM $(2f_c - 2B)$ is greater than the right edge of the third-order regrowth $(f_c + 3B)$. Thus, there is no overlap between the second-order IM and third-order regrowth, not to mention the passband spectrum. While in scenario 1, the second-order IM has no direct effects on either passband or adjacent bands, it might interfere with other applications far away from the passband. For example, if a 5G signal centred at 930 MHz (in downlink band n8 [15]) is transmitted, then the second-order IM will centre at 1860 MHz, which is in downlink n3. Thus, the interference generated from downlink band n8 will affect the applications in downlink n3.

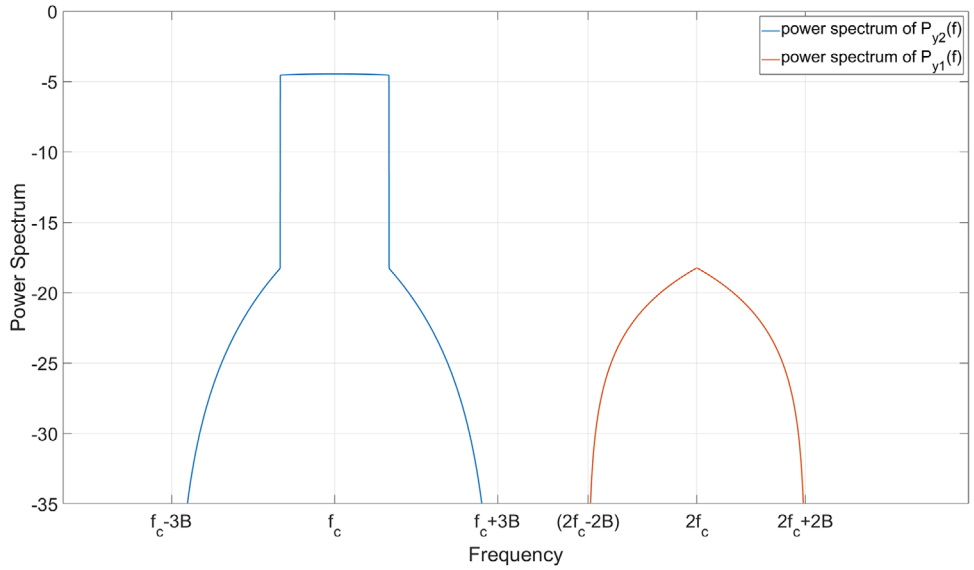

FIGURE 3 Power spectrum of $P_{y_1}(f)$ and $P_{y_2}(f)$ in scenario 1

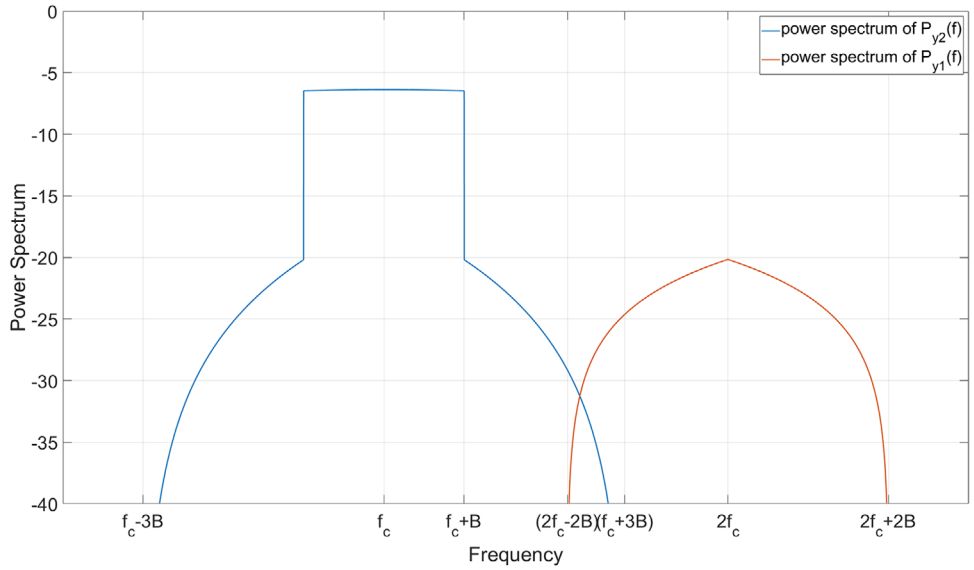

FIGURE 4 Power spectrum of $P_{y_1}(f)$ and $P_{y_2}(f)$ in scenario 2

3.2 | Frequency scenario 2

$$3B < f_c < 5B \tag{30}$$

This condition is derived from $f_c + B < 2f_c - 2B < f_c + 3B$. An illustration of scenario 2 is shown in Figure 4. This is a hypothetical example, which might be applicable to wireless applications other than 5G.

As shown in Figure 4, the left edge of the second-order IM ($2f_c - 2B$) falls into the third-order regrowth but has not reached the passband yet. Thus, there is an overlap between the second-order IM and third-order regrowth but no overlap between the second-order IM and the passband. In scenario 2, the second-order IM will degrade the adjacent channel leakage ratio performance by increasing the power of the adjacent channel, and such increased emission will potentially exceed the spectrum emission mask.

3.3 | Frequency scenario 3

$$f_c < 3B \tag{31}$$

This condition is from $2f_c - 2B < f_c + B$. However, Equation (31) is unlikely to happen in current wireless communications, as $f_c < 3B$ is rare. But this may happen in other standards. An illustration of scenario 3 is shown in Figure 5.

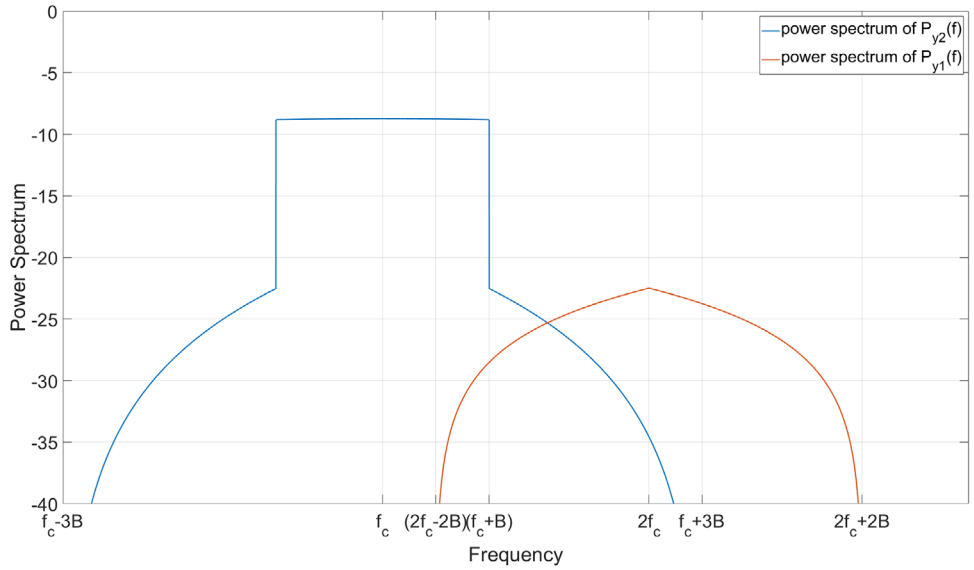

FIGURE 5 Power spectrum of $P_{y_1}(f)$ and $P_{y_2}(f)$ in scenario 3

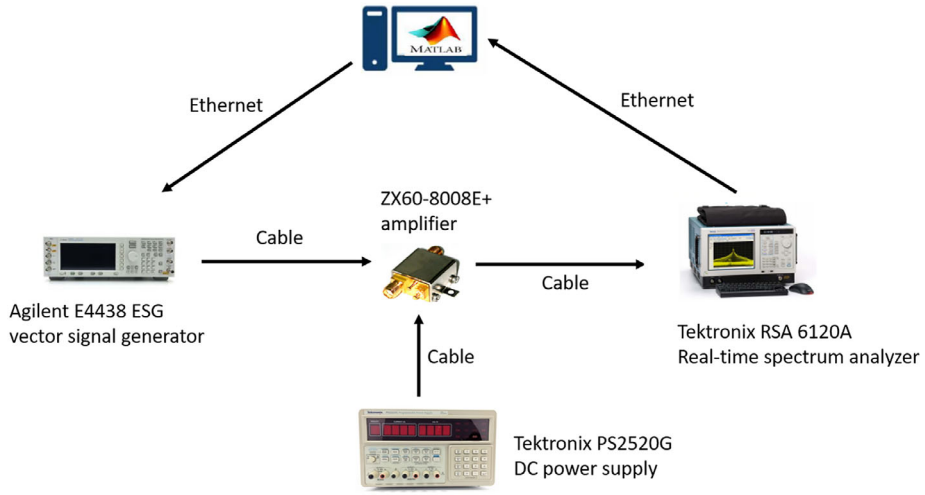

FIGURE 6 Experiment setup

As shown in Figure 5, the left edge of the second-order IM ($2f_c - 2B$) is less than the right edge of the passband ($f_c + B$), which means that there is overlap between the second-order IM and passband, not to mention the overlap between the second-order IM and third-order regrowth.

From the scenarios studied above, bandpass or bandstop filtering could be applied to eliminate the second-order interference in scenario 1, and predistortion technology should be considered to avoid the second-order regrowth in scenarios 2 and 3.

4 | EXPERIMENT VALIDATION

The experiment setup is described in Figure 6. An Agilent E4438 ESG vector signal generator is used to transmit an OFDM signal, which is coded using MATLAB, through a Mini-Circuit amplifier ZX60-8008E+. A Tektronix RSA 6120A real-time spectrum analyser is used to detect the amplified signal from the output of the amplifier. A Tektronix PS2520G DC power supply provides power for the amplifier.

In this experiment, the centre frequency of the OFDM signal is set at 930 MHz (f_c =930 MHz) with a bandwidth of 5 MHz (B = 5 MHz). These parameters are chosen from 5G NR frequency bands and channel bandwidths [15]. The IP_2 is measured as 38.69 dBm using a two-tone test at the same centre frequency [3]. The linear output powerP_0 is 1.5 dBm. Through the spectrum analyser, we can clearly observe the power spectrum of the second-order IM is located around the second-order harmonic frequency $2f_c$ =1860 MHz as expected. The measured and predicted power spectrum of the second-order IM in scenario 1 are shown in Figure 7.

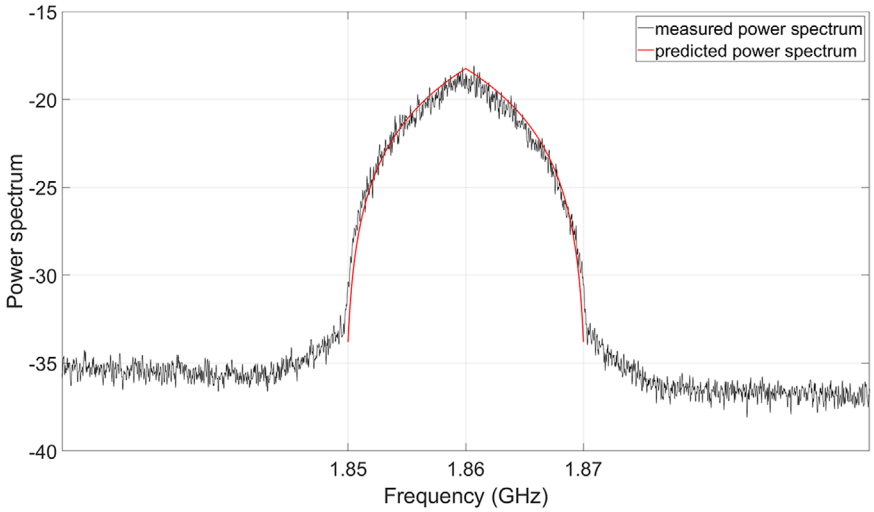

FIGURE 7 Measured and predicted power spectrum of the second-order IM in scenario 1

In Figure 7, the black waveform represents the power spectrum of measured second-order IM, and the red curve represents the power spectrum of predicted second-order IM. It is clearly shown that the predicted power spectrum matches the measured power spectrum.

5 | CONCLUDING REMARKS

In this article, the power spectrum model of the second-order IM is developed based on IP2, which is now starting to appear in datasheets, and other parameters. Using this model, RF professionals can easily predict the second-order IM spectrum and its interferences on different spectrum bands without conducting actual experiments or simulations, not to mention costly field trials.

We analysed three different frequency scenarios for passband of interest, for adjacent channels, and for other possible applications, in terms of the relation between the carrier frequency and bandwidth.

ORCID

Fu Li https://orcid.org/0000-0001-8819-0547

REFERENCES

1. Cripps, S.C.: RF Power Amplifiers for Wireless Communications, 2nd ed. Artech House, Inc, Norwood, USA (2006)
2. IP2 measurements of wideband amplifiers. https://www.everythingrf.com/whitepapers/details/3336-ip2-measurements-of-wideband-amplifiers (2020). Accessed 22 Dec 2020
3. Measuring the nonlinearities of RF amplifiers using signal generators and a spectrum analyzer. https://scdn.rohde-schwarz.com/ur/pws/dl_downloads/dl_application/application_notes/1ma71/1MA71_2e_amplifier_nonlin_meas.pdf (2020). Accessed 22 Dec 2020
4. Mahdi, A.E., Sobih, A.G., El-Kafafi, M.A.: Design and implementation of 10W, highly linear, wideband and efficient power amplifier using harmonic termination. In: 2016 IEEE Middle East Conference on Antennas and Propagation (MECAP), Beirut, pp. 1–4 (2016)
5. Kobayashi, K.W.: Bias optimized IP2 & IP3 linearity and NF of a decade-bandwidth GaN MMIC feedback amplifier. In: 2012 IEEE Radio Frequency Integrated Circuits Symposium, Montreal, QC, Canada, pp. 479–482 (2012)
6. Najari, O.E., Amborg, T., Alvandpour, A.: Wideband inductorless LNA employing simultaneous 2nd and 3rd order distortion cancellation. In: NORCHIP 2010, Tampere, pp. 1–4 (2010)
7. Gebhard, A., et al.: A robust nonlinear RLS type adaptive filter for second-order-intermodulation distortion cancellation in FDD LTE and 5G direct conversion transceivers. IEEE Trans. Microwave Theory Tech. 67(5), 1946–1961 (2019)
8. Sadjina, S., et al.: A survey of self-interference in LTE-advanced and 5G new radio wireless transceivers. IEEE Trans. Microwave Theory Tech. 68(3), 1118–1131 (2020)
9. Mini-circuits datasheet. MPGA-152+. https://www.minicircuits.com/pdfs/MPGA-152+.pdf (2020). Accessed 22 Dec 2020
10. Li, X., Tam, K.W., Li, F.: Statistical model of OFDM and its application in nonlinearity analysis of LTE-advanced systems. Int. J. Electron. Lett. 4(3), 296–301 (2015)
11. Couch, L.W.: Digital and Analog Communication System, 8th ed. 241–244. Pearson, New York, NY, USA (2013)
12. Wu, Q., Xiao, H., Li, F.: Linear RF power amplifier design for CDMA signals: A spectrum analysis approach. Microwave J. (1998)
13. Vignat, C.: A generalized Isserlis theorem for location mixtures of Gaussian random vectors. Stat. Probab. Lett. 82(1), 67–71 (2011)
14. Yan, S., Yang, X., Li, F.: Effect of even-order nonlinear terms on dual-band power amplifier modelling. Microwave Opt. Technol. Lett. 61, 163–166 (2019)
15. 3GPP specification series: 38series. https://www.3gpp.org/DynaReport/38-series.htm (2020) Accessed 22 Dec 2020

How to cite this article: Yang X, Li S, Yan S, Li F. On IP2 impact to nonlinear distortion of RF amplifiers. *J Eng.* 2021;1–7. https://doi.org/10.1049/tje2.12028